Study on the Unsteady Wakes Past a Square Cylinder near a Wall

Tae-yoon Kim
Professor, School of Mechanical and Aerospace Engineering in Seoul National University, Seoul, Korea
Bo-sung Lee
Senior Researcher, Korea Institute of Science and Technology Information, Daejeon, Korea
Dong-ho Lee*
Professor, School of Mechanical and Aerospace Engineering in Seoul National University, Seoul, Korea

Experimental and numerical studies on the unsteady wake field behind a square cylinder near a wall were conducted to find out how the vortex shedding mechanism is correlated with gap flow. The computations were performed by solving unsteady 2-D Incompressible Reynolds Averaged Navier-Stokes equations with a newly developed ε-SST turbulence model for more accurate prediction of large separated flows. Through spectral analysis and the smoke wire flow visualization, it was discovered that velocity profiles in a gap region have strong influences on the formation of vortex shedding behind a square cylinder near a wall. From these results, Strouhal number distributions could be found, where the transition region of the Strouhal number was at G/D=0.5~0.7 above the critical gap height. The primary and minor shedding frequencies measured in this region were affected by the interaction between the upper and the lower separated shear layer, and minor shedding frequency was due to the separation bubble on the wall. It was also observed that the position (y/G) and the magnitude of maximum average velocity (u/u_∞) in the gap region affect the regular vortex shedding as the gap height increases.

Key Words : Shedding Frequency, Separated Shear Layer, Separation Bubble, Vortex Shedding

Nomenclature

Roman Symbols

B : Breadth of cylinder
d : Length from the nearest wall
C_d : Coefficient of Drag
C_l : Coefficient of Lift
D : Height of cylinder
f : Shedding Frequency
F_1, F_2 : Blending Function
G : Gap height from the wall
k : Turbulent kinetic energy
Re : $u_\infty D/\nu$, Reynolds number
Rms : Root Mean Square
St : Df/u_∞, Strouhal number
u_∞ : Free-stream Velocity

Greek Symbols

δ : Boundary layer thickness
ν : Kinetic Viscosity
τ : Turbulent shear stress
ω : Specific Dissipation rate
ε : Dissipation rate

* Corresponding Author,
E-mail : donghlee@snu.ac.kr
TEL : +82-2-882-7927; **FAX** : +82-2-882-7927
Professor, School of Mechanical and Aerospace Engineering in Seoul National University, Seoul, Korea. (Manuscript **Received** October 8, 2004; **Revised** March 3, 2005)

1. Introduction

In the design stage of bluff bodies such as bridges, heavy ground vehicles, and open space buildings with support pillars on the ground floor, the dynamic stability of bodies must be considered due to unsteady wind loading. The flow around a bluff body is associated with flow separation, reattachment, and unsteady vortex formation in the wake region. As bluff bodies approach the ground, the vortex shedding is suppressed and becomes dependent on various parameters such as the Reynolds number, the Breadth-to-height ratio (B/D), the blockage ratio, the free-stream turbulence intensity and the incoming turbulent wall boundary layer thickness, etc (Durao, 1991).

Various studies on the flow field around a cylinder near a wall have been performed, but the results were unsatisfactory until now. Kenjo et al. (1997) reported for an experimental study for the flow around a two dimensional square cylinder mounted in the vicinity of a solid wall using the two-component Laser-Doppler Velocimetry (LDV) at Re=23,000 and $\delta/D=1.5$. They reported that the vortex shedding was suppressed at $G/D=0.25$ and that the Strouhal number increased, with decreasing gap height, from 0.133 at the freestanding condition to 0.164 at $G/D=0.3$. Bosch et al.(1996) carried out the experiment at Re=22,000, $\delta/D=0.8$ and reported that the regular vortex shedding did not occur at $G/D=0.25$, but the established shedding was observed at $G/D=0.5$. They reported that the critical gap height was in the range $G/D=0.35\sim0.5$, and there was no sharp transition from non-periodic flow to purely periodic flow. Lyn et al.(1995) performed the phase-averaged two-dimensional LDV measurements at Re=22,000 and 7% blockage ratio. For G/D=0.75 along one streamwise plane, it was observed that the wake flow was similar to that of the square cylinder in a uniform stream, but that the vorticies closer to the wall were distorted. Bailey et al.(2002) measured surface pressure and velocity field of a square cylinder near a wall at Re=19,000. They claimed that the straightening of the lower shear layer results in a weakened coupling between the upper and lower shear layers so that the shedding process becomes increasingly irregular at $G/D<0.6$. Martinuzzi et al.(2003) carried out the experiment at Re=18,900 and $\delta/D=0.5$, where the flow reattached intermittently on the bottom face of the cylinder and viscous effects became important at $0.3<G/D<0.6$.

From the viewpoint of computational fluid dynamics, it is difficult to predict accurately the unsteady turbulent flows with massive flow separation using the conventional turbulence models. Frank and Rodi (1991) showed that the Strouhal number and the drag coefficient of a square cylinder in a uniform flow could be predicted by the unsteady two-dimensional analysis using the Reynolds-stress equation model in combination with a wall function. Kato and Launder (1993) used the irrotationality of the flow at the impinging region and proposed the modified k-ε model, which is expressed in terms of the vorticity tensor and the velocity strain tensor. In addition, they applied this model to a square cylinder and could obtain the improved prediction of aerodynamic and turbulence statistics. Murakami et al.(1995) noted the excessive production of the turbulent kinetic energy due to the isotropic eddy viscosity model. Lee (1997) calculated the flow past a square cylinder by using the standard RNG (ReNormalization Group) and the low-Reynolds number k-ε model in order to evaluate the sensitivity of various parameters such as time accuracy, spatial accuracy and choice of convection schemes. Hwang et al.(1997) discovered that the Strouhal number decreased as the gap height increased at $\delta/D=0.8$, but the opposite phenomena occurred at $\delta/D=5.0$. They concluded that this result was due to the loss of momentum at the gap region as the wall boundary layer grew.

The objective of this study is to investigate the correlation between the velocity profile in the gap region and the unsteady wake behind a square cylinder as the gap height changes. For that, a new turbulence model (ε-SST) suggested will more accurately predict such unsteady wake flows. Also spectral analysis, flow visualization and the measurement of velocity profiles in the

gap region were performed to analyze the flow characteristics around the square cylinder.

This study is composed of two parts. In the fore part, the performance verification as well as the introduction of the ε-SST in the massive separated flow field will be discussed. Thereafter, in order to investigate the correlation between the velocity profile and the unsteady wake, the computational and experimental results will be mentioned in the latter part of this study.

2. ε-SST Turbulence Model

The BSL (baseline) model by Menter, utilizes the original k-ω model in the inner region of the boundary layer and the standard k-ε model in the outer region and free shear flows. It is similar to the k-ω model of Wilcox (1993), but avoids the strong free-stream sensitivity of the k-ω model (Menter, 1994).

To derive Menter's BSL model, the k-ε model is rewritten in a k-ω formulation. After multiplying a blending function F_1 to the original k-ω model, and $(1-F_1)$ to the transformed k-ε model, both equations are added together. Eq. (1) and (2) show BSL model suggested by Menter.

$$\frac{Dk}{Dt}=\tau_{ij}\frac{\partial u_i}{\partial x_j}-\beta^*\omega k+\frac{\partial}{\partial x_j}\left[(\nu+\sigma_k\nu_t)\frac{\partial k}{\partial x_j}\right] \quad (1)$$

$$\frac{D\omega}{Dt}=\frac{\gamma}{\nu_t}\tau_{ij}\frac{\partial u_i}{\partial x_j}-\beta\omega^2+\frac{\partial}{\partial x_j}\left[(\nu+\sigma_\omega\nu_t)\frac{\partial \omega}{\partial x_j}\right] +2(1-F_1)\sigma_{\omega_2}\frac{1}{\omega}\frac{\partial k}{\partial x_j}\frac{\partial \omega}{\partial x_j} \quad (2)$$

The left hand sides of Eq. (1) and (2) are the Lagrangian derivatives as noted $D/Dt=\partial/\partial t+u_i\partial/\partial x_i$ and the eddy viscosity of BSL model is defined as

$$\nu_t=\frac{k}{\omega} \quad (3)$$

The function F_1 is designed to be 1 to activate the original k-ω model in the near wall region and to be 0 from the surface to activate the standard k-ε model. The blending will take place in the wake region of the boundary layer. All constants denoted as ϕ in the BSL model are defined in Eq. (4) with blending function F_1. ϕ_1 represents any constant in the k-ω model while ϕ_2 is any constant in the transformed k-ε model (Menter, 1993).

$$\phi=F_1\phi_1+(1-F_1)\phi_2 \quad (4)$$

The blending function F_1 is given in the Eq. (5).

$$F_1=\tan h(\Lambda_1^4)$$

$$\Lambda_1=\min\left[\max\left(\frac{\sqrt{k}}{0.09\omega d},\frac{500\nu}{d^2\omega}\right),\frac{4\sigma_{\omega_2}k}{CD_{k\omega}d^2}\right] \quad (5)$$

In the first term in Eq. (5), turbulence length scale is divided by d, the length from the nearest wall. It is equal to 2.5 in the log layer and 0 in the boundary layer edge. The second term is designed to ensure that F_1 is equal to 1 in the sub-layer. The third term is used to remove the strong free-stream dependency when ω has a very low value. Therefore Λ_1 becomes 0 near the boundary layer edge, and the standard k-ε model is activated.

$$CD_{k\omega}=\max\left(2\sigma_{\omega_2}\frac{1}{\omega}\frac{\partial k}{\partial x_j}\frac{\partial \omega}{\partial x_j},\ 10^{-20}\right) \quad (6)$$

$CD_{k\omega}$ stands for the positive portion of the cross-diffusion term appeared in Eq. (2).

In addition to the BSL model, which combines the standard k-ε model and the k-ω model, Menter suggested an improved turbulence model called the SST (Shear Stress Transport) model. In the SST model, the eddy viscosity is modified to account for the transport of the principal turbulent shear stress denoted as

$$\tau=-\rho\overline{u'v'} \quad (7)$$

One of the major differences between eddy-viscosity and full Reynolds-stress model is that the latter accounts for the transport effect of the principal turbulent shear stress. The importance of this effect has been clearly demonstrated by the success of the Johnson-King (JK) model which shows significantly improved results for adverse pressure gradient flows (Menter, 1994). The JK model suggests a transport equation for the turbulent shear stress τ, which is based on Bradshaw's assumption that the shear stress in a boundary layer is proportional to the turbulent kinetic energy k, as in Eq. (8), where a1 is a constant of 0.31.

$$\tau=\mu_t\left(\frac{\partial u}{\partial y}\right)=\rho a_1 k \tag{8}$$

On the other hand, in the two-equation model, the turbulent shear stress is written as Eq. (9).

$$\tau=\mu_t\left(\frac{\partial u}{\partial y}\right)=\rho C_\mu\frac{k^2}{\varepsilon}=\rho\frac{k}{\omega}\left(\frac{\partial u}{\partial y}\right) \tag{9}$$

And, Eq. (9) can be rewritten as Eq. (10) for conventional two-equation models.

$$\tau=\rho\sqrt{\frac{P_k}{D_k}}a_2 k \tag{10}$$

To ascertain an equilibrium turbulent boundary layer flow, the ratio of production (P_k) to dissipation (D_k) in Eq. (10) is close to 1 in the outer part of the layer. Therefore, Eq. (10) satisfies Eq. (8), which represents Bradshaw's assumption.

In adverse pressure gradient flows, the ratio of production (P_k) to dissipation (D_k) can be significantly larger than unity ($P_k \gg D_k$). As a result, Eq. (10) leads to an over-prediction of turbulent shear stress, hence in order to satisfy Bradshaw's assumption, the eddy viscosity in the SST model is redefined as in Eq. (11) where the P_k to D_k ratio is unity.

$$\nu_t=\frac{a_1 k}{\max[a_1\omega,\ (\partial u/\partial y)F_2]} \tag{11}$$

F_2, another blending function, varies from 0 in the free shear layer to 1 in the boundary layer flow. The blending function F_2 is defined as follows.

$$F_2=\tanh(A_2^2) \tag{12}$$

$$A_2=\max\left(2\frac{\sqrt{k}}{0.09\omega d},\ \frac{500\nu}{d^2\omega}\right) \tag{13}$$

In the boundary layer with adverse pressure gradient, the production of k is larger than the dissipation (or $\partial u/\partial y > a_1\omega$). Then, Eq. (11) guarantees the satisfaction of Eq. (8) due to $\nu_t=a_1 k/(\partial u/\partial y)$. Whereas the original formulation such that $\nu_t=k/\omega$ is used for the rest of the flow. In the original SST model, the eddy-viscosity can be generalized using the absolute value of vorticity as shown in Eq. (14). In two-dimensional flows, $|\Omega_{ij}|$ is defined as Eq. (15).

$$\nu_t=\frac{a_1 k}{\max(a_1\omega,\ 2|\Omega_{ij}|F_2)} \tag{14}$$

$$|\Omega_{ij}|=\sqrt{2\Omega_{ij}\Omega_{ij}}=\frac{1}{2}\left|\frac{\partial u}{\partial y}-\frac{\partial v}{\partial x}\right| \tag{15}$$

The SST model has been validated for various steady and unsteady turbulent flow fields (Ekaterinaris, 1994) and is known to show results superior to other eddy viscosity turbulence models. However, it has been observed that there are some discrepancies in predicting unsteady aerodynamic coefficients in massive separation regions such as the oscillating airfoil (Menter, 1994) and the square cylinder (Kim, 2003).

Ekaterinaris (1994) explained that this numerical oscillation at post-stall region with the SST model resulted from vortex shedding at the wake region, which was influenced by grid distribution at the trailing edge and wake region. However, the present study clarifies that fluctuation of aerodynamic coefficients results from the SST turbulence model itself and aims to provide better results by enhancing the SST model based on the replacement of the vorticity tensor with the strain rate tensor.

At first, the shear stress of two-equation model of Eq. (9) can be derived from Eq. (16) which is the basic premise of eddy viscosity model that shear stress tensor τ_{ij} is proportional to strain tensor S_{ij}.

$$\tau_{ij}=\mu_t\left(\frac{\partial u_i}{\partial x_j}+\frac{\partial u_j}{\partial x_i}-\frac{2}{3}\frac{\partial u_k}{\partial x_k}\delta_{ij}\right)-\frac{2}{3}\rho k\delta_{ij} \tag{16}$$

In two-dimensional flows, Eq. (16) can be represented as follows;

$$\begin{aligned}\tau_{xy}&=2\mu_t S_{xy}=\mu_t\left(\frac{\partial u}{\partial y}+\frac{\partial v}{\partial x}\right)\\&=\rho\frac{k}{\omega}\left(\frac{\partial u}{\partial y}+\frac{\partial v}{\partial x}\right)\end{aligned} \tag{17}$$

From Eq. (17), the eddy viscosity of the SST turbulence model is redefined as follows,

$$\begin{aligned}\nu_t&=\frac{a_1 k}{\max\left[a_1\omega,\ \left(\frac{\partial u}{\partial y}+\frac{\partial v}{\partial x}\right)F_2\right]}\\&=\frac{a_1 k}{\max(a_1\omega,\ 2S_{xy}F_2)}\end{aligned} \tag{18}$$

$$\nu_t=\frac{a_1 k}{\max(a_1\omega,\ 2|S_{ij}|F_2)} \tag{19}$$

In two-dimensional flows, $|S_{ij}|$ is defined as Eq. (20).

$$|S_{ij}|=\sqrt{2S_{ij}S_{ij}}=\frac{1}{2}\left|\frac{\partial u}{\partial y}+\frac{\partial v}{\partial x}\right| \tag{20}$$

When the streamlines are nearly parallel to the solid surface as in the attached boundary layers or weak separation, $(\partial u/\partial y)$ is much larger than $(\partial v/\partial x)$. Hence, the shear stress in Eq. (17) can be simplified as Eq. (9) by neglecting the latter term $(\partial v/\partial x)$. However, Eq. (17) cannot be simplified as Eq. (9) in large separation region because the streamlines are no longer parallel to the surface.

Therefore, $(\partial v/\partial x)$ cannot be neglected any longer when the large separation occurs in Eq. (18). For general flows including the attached flows without separation and the large separated flows, the eddy-viscosity can be redefined as shown in Eq. (19) using the absolute value of strain rate $|S_{ij}|$.

In this study, to distinguish the new turbulence model from the original SST model, the new turbulence model is referred to the ε-SST (the enhanced SST) model.

Figure 1 shows the schematic comparison of vorticity tensor and strain tensor appeared in the eddy viscosity formulation both in case of weak and large separations. If the large separation occurs as in Fig. 1, the sign of $(\partial u/\partial y)$ and $(\partial v/\partial x)$ are opposite and the magnitude of $|S_{ij}|$ is always less than $|\Omega_{ij}|$. Therefore, the quantities of denominators in the eddy viscosities of each

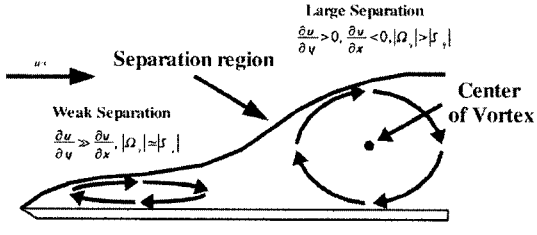

Fig. 1 Schematic comparison of vorticity tensor and strain rate tensor

model can be represented as follows,

$$a_1\omega<\frac{1}{2}\left|\frac{\partial u}{\partial y}+\frac{\partial v}{\partial x}\right|<\frac{1}{2}\left|\frac{\partial u}{\partial y}-\frac{\partial v}{\partial x}\right| \tag{21}$$

According to Eq. (21), the eddy viscosities of each model in large separated flows satisfy the following relationship;

$$\nu_{t(k-\varepsilon)}>\nu_{t(\varepsilon\text{-SST})}>\nu_{t(\text{SST})} \tag{22}$$

Because the order of $(\partial v/\partial x)$ is much less than that of $(\partial u/\partial y)$ in the attached flow region or the weak separation region, the absolute values of the vorticity tensor and the strain rate tensor have almost the same order of magnitude.

Previous studies (Menter, 1994) using the original SST turbulence model show reasonable predictions because those calculations were performed for attached and weak separation flows. However when large separated regions exist, the magnitude of the eddy viscosity in the original SST model is much less than what is expected. Therefore, the insufficient dissipation results in the oscillation in the large separated flow fields as previously mentioned (Ekaterinaris, 1994; Kim, 2003).

The effects of replacement of the vorticity tensor with the strain rate tensor in the eddy viscosity definition will be evaluated by the large separated flow region such as a square cylinder flow. From this evaluation, it will be validated that the ε-SST model shows better prediction capability in the unsteady large separated flow fields than the original SST model and the most other models. The numerical analysis condition is chosen as Re=22,000 to match the experimental condition (Lyn, 1994) and Large-Eddy Simulation (Murakami, 1995). Table 1 summarizes the mean aerodynamic coefficients from different turbulence models - the standard k-ε, the BSL, the SST and the ε-SST turbulence model - in terms of the Strouhal number and the aerodynamic lift and drag coefficients. The results from the ε-SST turbulence model are in good agreement with the experimental result (Lyn, 1994) and LES result (Murakami, 1995), although the lift coefficient is slightly over predicted compared to the LES result.

Table 1 Numerical parameters and results with various turbulence models

Model	Δt	Δx_i	C_l	C_d	St
k-ε [Lee, 1997]	0.02	0.035	0.56	1.75±0.004	0.138
RNG k-ε [Lee, 1997]	0.02	0.035	2.08	2.12×0.230	0.133
Low Re k-ε [Lee, 1997]	0.02	0.0012	1.61	2.10±0.040	0.134
LES [Murakami, 1995]	0.001	0.022	1.60	2.09±0.130	0.132
EXP [Lyn, 1994]	-	-	-	2.14±0.090	0.134
k-ε [Present]	0.05	0.005	1.04	1.90±0.054	0.138
BSL [Present]	0.05	0.005	1.40	2.00±0.064	0.142
SST [Present]	0.05	0.005	2.36	2.13×0.358	0.123
ε-SST [Present]	0.05	0.005	2.01	2.01±0.187	0.131

Figure 2 shows the time averaged U velocity component along the centerline. The SST model yields an excessively narrow reverse flow region compared to the experimental result and LES result. The result obtained from the ε-SST turbulence model is well in accord with the LES result although it is found to be narrow compared to the experimental result. The size of the reversed flow region from the standard k-ε model is larger than the other results. The differences in the estimated size of the reversed flow region may be due to the different magnitude of turbulent mixing in the wake of the square cylinder, which is illustrated as the total kinetic energy in Fig. 3. Total turbulent kinetic energy, which is the sum of the stochastic and the periodic kinetic energy, is shown in Fig. 3, where all the computations deviate from the experimental result. Though Lyn's experiment was performed by 2-D modeling, the TKE that was measured also included spanwise kinetic energy not appeared in numerical computations Therefore, the TKE of the experiment is higher than LES and RANS with the turbulence models. The ε-SST model somewhat under-predicts the periodic part and the stochastic part, while the location of peak TKE coincides with the LES and Lyn's experiment. The SST model is similar to the ε-SST model in the stochastic part, but over-predicts in the periodic part and the location of peak TKE is closer to the wall than other models. The BSL and the standard k-ε model under-predict both parts. The periodic part can be related to the turbulent

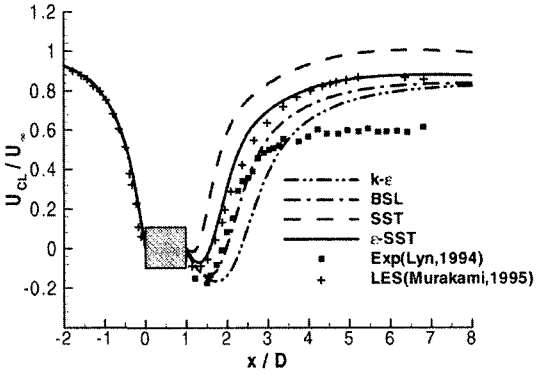

Fig. 2 Time averaged velocity component along the centerline of the square cylinder (Free-standing, Re=22,000)

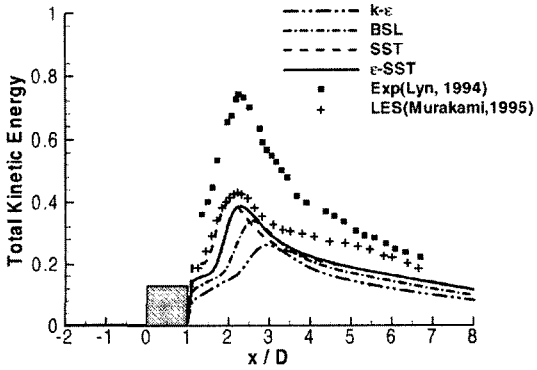

Fig. 3 Time averaged TKE along the centerline of the square cylinder (Free-standing, Re= 22,000)

mixing in the wake of the square cylinder and the size of the wake, therefore the peak TKE location of the SST is closest to the square cylinder. Far

from the square cylinder, the ε-SST prediction of the stochastic part is in agreement with that of the SST. By comparing turbulence statistics with the Lyn's experiment and Murakami's LES, the ε-SST turbulence model is found to reproduce important flow features around the square cylinder.

3. Numerical Approach

In this study, governing equations are 2-D unsteady incompressible Reynolds-averaged Navier-Stokes equations. To calculate incompressible flow fields with efficiency, the continuity equation was transformed to the pressure equation with the pseudo-compressibility scheme (Rogers, 1990). Then, the governing equations are given as

$$\frac{\partial p}{\partial t_c}=-\beta\frac{\partial u_i}{\partial x_i} \tag{23}$$

$$\frac{\partial u_i}{\partial t_c}+\frac{\partial u_i u_j}{\partial x_j} =-\frac{\partial p}{\partial x_i}+\frac{\partial}{\partial x_j}\left[(\nu+\nu_t)\left(\frac{\partial u_i}{\partial x_j}+\frac{\partial u_j}{\partial x_i}\right)\right]-\frac{\partial u_i}{\partial t} \tag{24}$$

The third-order upwind biased scheme was employed for the convection terms, and the central difference scheme was used for the viscous terms. To calculate the time-dependent flow fields, dual time stepping method was employed, where physical time terms were treated as sources at the right hand side as shown in Eq. (24). The numerical calculation procedure at each physical time step Δt became the same with that of steady-state solution. Parallel computing was employed for effective analysis of unsteady flows. To this end, physical domain was divided into several subdomains by using DDT (domain decomposition technique). DP-SGS (Data Parallel Symmetric Gauss-Seidel) (Lee, 1997) method developed for efficient parallel computing was employed for temporal integration. At Fig. 4, D and B indicate respectively height and breadth of the cylinder and G means gap height from the ground. At the inflow, 1/7 power law with the adequate boundary layer thickness ($\delta/D=1.23$) was imposed at 10D in front of the rectangular cylinder. At the outlet, flow properties were extrapolated and symmetric boundary conditions were imposed. On the upper boundaries and no-slip boundary, conditions were imposed on the cylinder wall surface and ground. To investigate the effects of the grid size and the first grid spacing on the numerical solutions, grid independency tests were carried out at $G/D=1.0$ case with 398×298 grid where the first grid spacing $\Delta x_i/D=0.0025$, 198×148 where $\Delta x_1/D=0.005$, and 98×73 where $\Delta x_i/D=0.01$. The effect of the physical time step on the unsteadiness of the solution was also investigated with $\Delta t=0.025$, 0.05, 0.1 cases in 198×148 grid. Table 2 summarizes the preliminary test results, and concludes that the 198×148 grid and $\Delta t=0.05$ are sufficient for the following numerical experiments in view of them being nearly identical with the Strouhal numbers and aerodynamic coefficients from 198×148 and 398×298 grid.

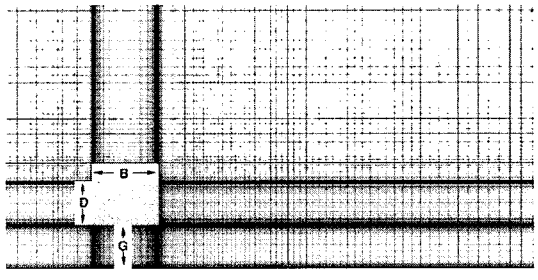

Fig. 4 H-type 1-blcok grid system (198×148, $\Delta x_i/D=0.005$)

Table 2 Numerical parameters and results with various grids and time steps

Grid size	Δt	Δx_i	C_l	C_d	St
98×73	0.05	0.01	$-1.68\sim2.10$	$1.61\sim1.98$	0.126
198×148	0.1	0.005	$-1.98\sim1.93$	$1.80\sim2.07$	0.149
198×148	0.05	0.005	$-2.02\sim1.97$	$1.78\sim2.25$	0.153
198×148	0.025	0.005	$-2.04\sim1.99$	$1.77\sim2.27$	0.154
398×298	0.05	0.0025	$-2.10\sim2.06$	$1.83\sim2.32$	0.152

4. Experimental Apparatus

The present study was performed in the subsonic wind tunnel with cross section of 300 mm × 200 mm with a length of 1,000 mm each, and the maximum speed was about 30 m/s and turbulence intensity was less than 0.5%. The flow situation and the coordinate system used in this study are sketched in Fig. 5. The test model was a two-dimensional square cylinder made of acryl, of height D=26 mm and span of 7.7D, resulting in a blockage ratio of approximately 10%. The cylinder was horizontally mounted with a 1-axis traverse unit at 21D downstream of the plate leading edge. In order to remove the wall boundary layer from the bottom of the test section, the test section was divided by a horizontal partition plate that was installed at the bottom. The plate had a super-critical shape in leading edge for a uniform velocity profile. The trip wires of various diameters were installed in front of the horizontal partition plate in order to control the turbulent wall boundary layer thickness. The average inflow velocity was set to be u_∞=10.3 m/s, hence Re=18,000 (based on the on-coming velocity, u_∞, and the cylinder height, D) and a sampling frequency was 1 kHz. In order to observe the flow pattern of the unsteady wake region the smoke wire visualization technique was used. A Hot-Wire Anemometer (HWA, hereafter) was used to obtain the shedding frequency and to measure velocity profiles in the gap region. The uncertainty of free stream velocity was 0.5%. The large sampling time could minimize the uncertainty to less than ±0.001 in the gap flow region. The Strouhal number had the uncertainty of ±0.003.

From several preliminary experiments and numerical simulations performed with different boundary layer thicknesses, it was found that the relation between the velocity profile and the vortex shedding has similar qualitative characteristics as the boundary layer thickness changes. The present work has only chosen the experiments and numerical data at δ/D=1.23 and Re=18,000 to investigate those effects.

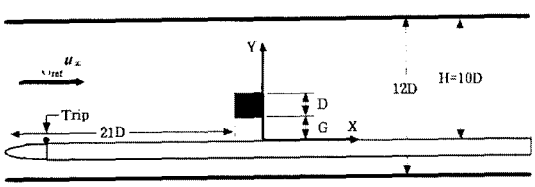

Fig. 5 Description of experimental setup

5. Results and Discussion

5.1 Flow pattern

The smoke wire technique was used to visualize the vortex shedding motion for various gap heights in the range of G/D=0~1.5 at δ/D=1.23 and Re=3,500 (u_∞=2 m/s). Okajima (1992) reported that the similar flow pattern around a square cylinder was detected in the wide range of Reynolds number between 100 and 20,000. From Okajima's result, the flow visualization results with smoke wire at Re=3,500 can simulate the flow pattern at Re=18,000. In Fig. 6, the instantaneous flow with smoke wire shows the similar flow pattern to the numerical simulation as shown in Fig. 7. At G/D=0.3 in Fig. 6, there is no regular vortex shedding because the gap flow between the square cylinder and the wall is squeezed like a jet flow, hence the lower separated shear layer can not interact with the upper separated shear layer of the cylinder. The vortex

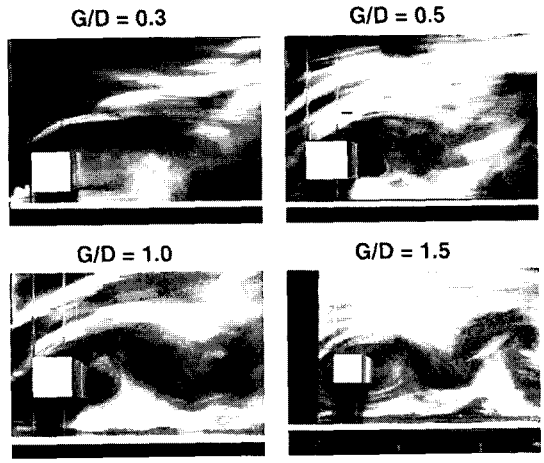

Fig. 6 Smoke wire flow visualization for various gap heights (δ/D=1.23, Re=3,500, u_∞=2 m/s)

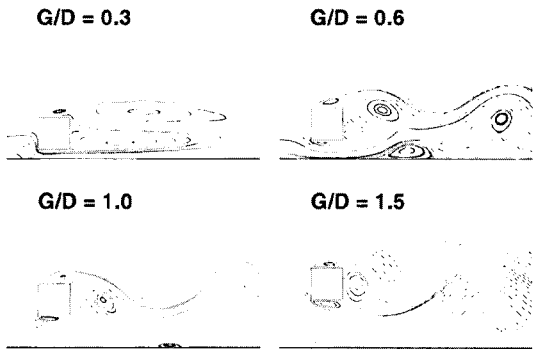

Fig. 7 Instantaneous streamline distributions for various gap heights (Computation, $\delta/D=1.23$, Re=18,000)

shedding occurs above $G/D=0.5$ where the sufficient momentum is furnished from the gap region to wake region as the gap height increases. The critical gap height may exist around $G/D=0.5$ where the intermittent vortex shedding is identified. At $G/D=1.0$ and 1.5, the Karman vortex streets appears to be slightly oblique due to the interference of separated shear layer on the ground.

Figure 7 shows instantaneous streamline distributions for various gap heights. At $G/D=0.3$, where the vortex shedding is suppressed, the long recirculation zone is identified past the square cylinder. But at $G/D=0.6$ above the critical gap height, the additional separation bubble that affects the wake region on the ground is identified. As the gap height increases, the separation bubble on the ground gets weaker and finally disappears at $G/D=1.5$.

5.2 Spectral analysis and strouhal number

Figure 8 shows the variation of lift coefficients at $G/D=0.6$, 0.7 and 1.0. When G/D is above 0.6, periodic oscillations are observed in Fig. 8. It is found that the lift coefficient has one primary shedding frequency and minor shedding frequencies at $G/D=0.6$ and 0.7. The primary shedding frequency is affected by the interaction between the upper separated shear layer and the lower separated shear layer of the square cylinder, and the minor shedding frequency is originated from interference of the separation bubble on the ground.

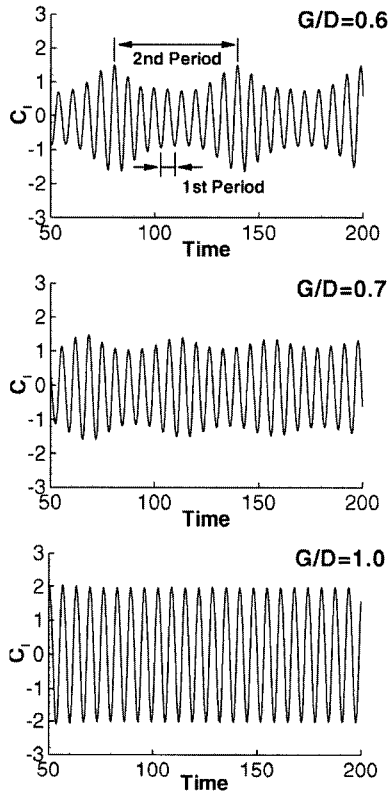

Fig. 8 Lift coefficients for various gap heights (Computation, $\delta/D=1.23$, Re=18,000)

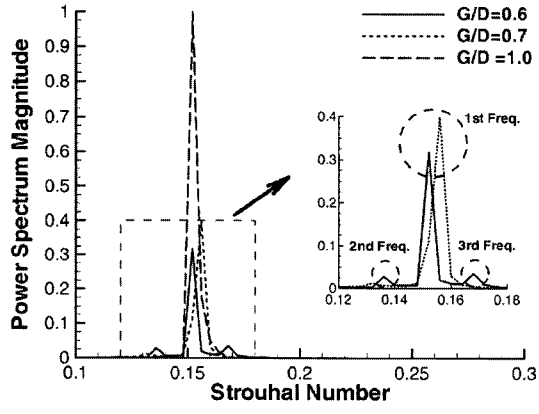

Fig. 9 FFT results of lift coefficients for various gap heights (Computation, $\delta/D=1.23$, Re=18,000)

It is also evident with the frequency domain in Fig. 9 and averaged streamline in Fig. 10. As the gap height increases, the separation bubble on the ground is weakened and finally the minor

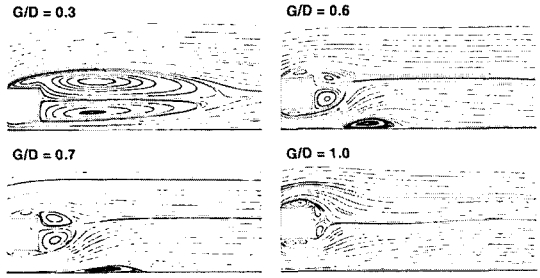

Fig. 10 Averaged streamline distributions for various gap heights (Computation, $\delta/D=1.23$, Re=18,000)

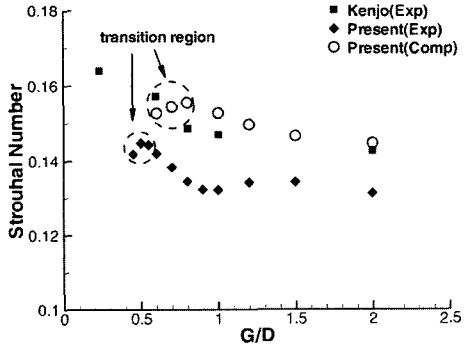

Fig. 11 Strouhal number distributions (Kenjo, 1997; $\delta/D=1.5$, Re=23,000, Present Experiment and Computation; $\delta/D=1.23$, Re=18,000)

shedding frequency disappears at $G/D=1.0$ as illustrated in Fig. 8. This phenomenon is confirmed by the moving ground (Kim, 2005) that the separation bubble does not exist. At $G/D=0.3$ in Fig. 10, a long circulation zone without vortex shedding is identified, however there is a separation bubble on the ground at $G/D=0.6$ and 0.7.

In Fig. 11, the Strouhal number that gap heights increases is compared with the results from Kenjo (1997). The transition region of the Strouhal number is found after the critical gap height in the present study, but Kenjo's result shows that the Strouhal number monotonically decreases as the gap height increases. This difference may be due to the increase of intermittent of the vortex shedding at $0.5<G/D<0.7$ as mentioned by Bailey et al.(2002) and Bosch et al. (1996) The present numerical simulation results are in good agreement with Kenjo's experimental

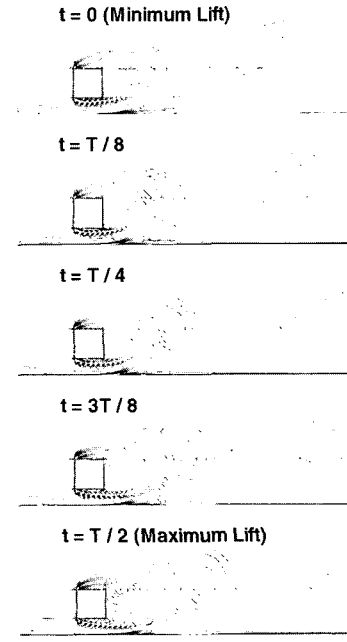

Fig. 12 Vortex formation process in a half cycle of oscillation at $G/D=0.6$ (Computation, $\delta/D=1.23$, Re=18,000)

result. The Strouhal number decreases and converges to the value at free standing as the gap height increases.

Figure 12 shows the vorticity contours during a half cycle of the vortex shedding formation at $G/D=0.6$. The periodic vortex shedding and the clockwise separated shear layer from the ground are clearly identified, and the vortex is upwardly inclined by the ground effect as seen at Fig. 6. The vortex at the lee side of the square cylinder is deflected because of the ground effect.

5.3 Velocity profiles in gap region

From the results given in the previous section, we can deduce that the gap flow and the separation bubble on the ground affect the vortex shedding behind the square cylinder near the ground. Therefore, it is important to investigate the velocity profiles in the gap region in order to understand the vortex formation mechanism. The averaged streamwise velocity distributions from computations and experiments are measured at the exit position of the gap between square cylinder and ground. Figure 13 and Figure 14 show

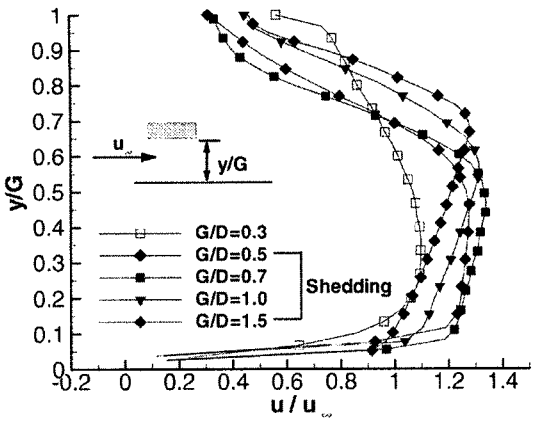

Fig. 13 Averaged velocity profile for various gap heights (Experiment, $\delta/D=1.23$, Re=18,000, Solid ; Vortex shedding, Blank ; Suppression)

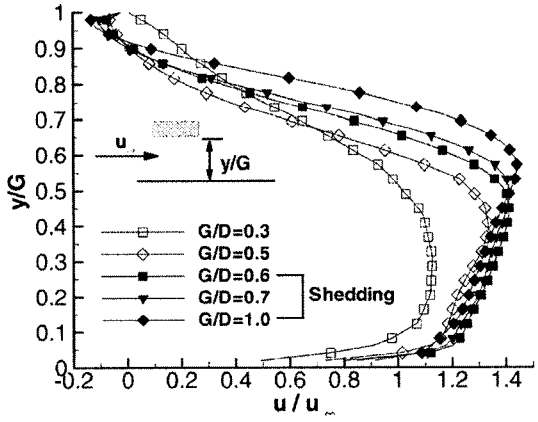

Fig. 14 Averaged velocity profile for various gap heights (Computation, $\delta/D=1.23$, Re=18,000, Solid ; Vortex shedding, Blank ; Suppression)

the averaged velocity profiles by experiments as well as the computation results for various gap heights. In the cases where the vortex shedding occurs, the value of maximum velocity denoted u/u_∞ is greater than the cases without vortex shedding. Also, the position at which maximum velocity occurs is closer to the lower surface of the square cylinder. If the square cylinder is located near the ground, the gap flow plays a role as a jet flow along the ground, causing the position (y/G) of maximum velocity to move closer to the ground. This deters interaction between the upper

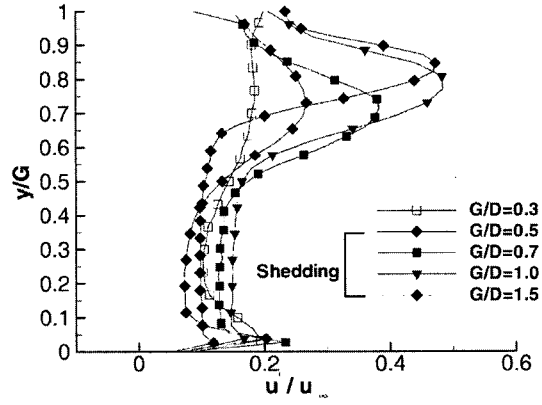

Fig. 15 Rms velocity profile for various gap heights (Experiment, $\delta/D=1.23$, Re=18,000, Solid ; Vortex shedding, Blank ; Suppression)

separated shear layer and the gap region flow, resulting in the suppression of the vortex shedding. The difference in the velocity profile between the experimental results and computational results seems to be due to the different turbulent intensity and the 3-D effect of the experimental conditions. Yet, the patterns of velocity profile in the present study are still meaningful from a qualitative analysis viewpoint.

Figure 15 shows the rms velocity profiles at $G/D=0.3\sim1.5$. In the case that the regular vortex shedding occurs, the position (y/G) of maximum rms value is higher than 0.6. At $G/D=0.5$, where intermittent vortex shedding exists. The averaged velocity profile shows the same tendency with $G/D=0.7$, 1.0 and 1.5 ; however the rms velocity profile is different from $G/D=0.7$, 1.0, 1.5. Therefore, the averaged and the rms velocity profiles are another base the intermittent vortex shedding occurs around $G/D=0.5$. With higher value of rms velocity, the more kinetic energy is furnished to the wake region. As the position of the maximum rms velocity approaches the lower surface of cylinder, there is more active interaction between the separated shear layers. Therefore, from these results, it is concluded that the position of maximum velocity (y/G) takes a key role in the unsteady oscillation past a square cylinder. Based on this investigation, simple passive control methods attached vertical or horizontal plates on the lower surface of the square

cylinder are helpful to reduce the aerodynamic drag as well as to suppress the vortex-induced oscillation. (Lee, 2005)

6. Conclusions

In this study, the unsteady flow field past a square cylinder near a wall has been investigated by experiments and numerical simulations. In order to verify the ε-SST turbulence model where is adapted for predicting large separation region such as a square cylinder, the 2-D incompressible Reynolds Averaged Navier-Stokes equations were used. Through spectral analysis and smoke wire flow visualization, it was discovered that the velocity profiles in a gap region have a strong influence on the vortex shedding past the square cylinder near a wall. The Strouhal number has a transition region around $G/D=0.5\sim0.7$ above the critical gap height. The primary shedding frequency is affected by the interaction between the upper and lower separated shear layers of the square cylinder. The minor shedding frequency originates from the separation bubble on the wall above the critical gap height. The pair vortex past a square cylinder near a wall was asymmetric and deflected upwards due to separated shear layer from the wall and the separation bubble. But these phenomena disappear as the gap height increases because the wall effect diminishes. The periodic vortex shedding mechanism has a strong correlation with the position (y/G) of maximum averaged and rms velocity (u/u_∞) in the gap region as well as the velocity itself. As the position of maximum velocity approaches the lower surface of cylinder, regular vortex shedding occurs. It is possible to suppress vortex shedding past a square cylinder near a wall by controlling the position of the maximum velocity and momentum in the gap region using various methods.

Acknowledgments

This work was supported by "the Brain Korea 21 Project in 2005" and "the Sixth Strategic Supercomputing Support Program in KISTI." Especially Tae-yoon Kim among the authors would like to appreciate advice of Prof. K. H. Kim.

References

Atsushi Okajima, 1982, "Strouhal Numbers of Rectangular Cylinders," *J. Fluid Mech.*, Vol. 123, pp. 379~398.

Bailey, S. C. C., Kopp, G. A. and Martinuzzi, R. J., 2003, "Vortex Shedding from a Square Cylinder near a Wall," *J. Turbulence*, paper 003, pp. 1~18.

Bhattacharyya, D. and Maiti, D. K., 2004, "Shear Flow past a Square Cylinder near a Wall," *Int. J. Eng. Sci.*, Vol. 42, pp. 2119~2134.

Bearman, P. W., Zdravkovich, M. M. 1978, "Flow around a Circular Cylinder Near a Plane Boundary," *J. Fluid Mech.*, Vol. 89, part 1, pp. 33~47.

Bosch, G., Kappler, M. and Rodi, W., 1996, "Experiments on the Flow Past a Square Cylinder Placed near a Wall," *Exp. Thermal Fluid Sci.*, Vol. 13, pp. 292~305.

David C. Wilcox, Turbulence Modeling for CFD, DCW Industries, Inc. 1993.

Durao, D. E. F., Gouveia, P. S. T. and Pereira, J. C. F., 1991, "Velocity Characteristics of the Flow around a Square Section Cylinder Placed near a Channel Wall," *Exp. in Fluids*, Vol. 11, pp. 341~350.

Frank, R. and Rodi, W., 1991, "Calculation of Vortex Shedding past a Square Cylinder with various Turbulence Models," *8th Symp. Turbulent Shear Flows*, Technical Univ. of Munch, 20-1.

Kato, M. and Launder, B. E., 1993, "The Modeling of Turbulent Flow around Stationary and Vibrating Square Cylinders," *9th Symp. Turbulent Shear Flows*, Kyoto Japan.

Kenjo, C. Q. Wu and Robert J. Martinuzzi, 1997, "Experimental Study of the Turbulent Wake Flow behind a Square Cylinder Near a Wall," *ASME, FEDSM* 97-3151.

Kim, T. Y., Lee, B. S., Lee, D. H. and Lee, D. H., 2003, "A Study on Vortex Shedding Around a Bluff Body Near the Ground," *SAE Paper*, 2003-01-1652.

Kim, T. Y., Lee, B. S. and Lee, D. H., "Numerical Analysis of the Vortex Shedding past a Cylinder with Ground Effect," *KSASS in Korea* (submitted)

Lee, B. S. and Lee, D. H., 1997, "Data Parallel Symmetric Gauss-Seidel Algorithm for Efficient Distributed Computing," *AIAA*, 97-2138.

Lee, B. S., Kim, T. Y. and Lee, D. H., "Control of Vortex Shedding behind a Rectangular Cylinder near the Ground," *Numerical Heat Transfer, Part A*, 47, Issue 9.

Lee, S. S., 1997, "Unsteady Aerodynamic Force Prediction on a Square Cylinder using k-ε Turbulence Models," *J. of Wind Eng. Ind. Aerodyn.*, Vol. 67&68, pp. 79~90.

Lee, S. S., 1997, "Spatial Resolution Effects on Unsteady Turbulent Flow Computations for the Rectangular Cylinders by k-ε Turbulence Models," *KSME Int.*, Vol. 11, No. 3, pp. 339~347.

Lyn, D. A. and Rodi, W., 1994, "The Flapping Shear Layer Formed by Flow Separation From the Forward Corner of a Square Cylinder," *J. Fluid Mech.*, Vol. 267, pp. 353~376.

Lyn, D. A., Einav, S., Rodi, W. and Park, J. H., 1995, "A Laser-Doppler Velocimetry Study of Ensemble-Averaged Characteristics of the Turbulent near Wake of a Square Cylinder," *J. Fluid Mech.*, Vol. 304, pp. 285~319.

Menter, F. R., 1994, "Two-Equation Eddy-Viscosity Turbulence Models For Engineering Applications," *AIAA J*, Vol. 32, No. 8, pp. 1598~1605.

Murakami, S. and Mochida, A., 1995, "On Turbulent Vortex Shedding Flow Past 2D Square Cylinder Predicted Flow Past 2D Square Cylinder Predicted by CFD," *J. of Wind Eng. Ind. Aerodyn.*, Vol. 54, pp. 191~211.

Park, W. C. and Higuchi, H., 1998, "Numerical Investigation of Wake Flow Control by a Splitter Plate," *KSME Int.*, Vol. 12, No. 1, pp. 123~131

Robert R. Hwang and Chia-Chi Yao, 1997, "A Numerical Study of Vortex Shedding From a Square Cylinder With Ground Effect," *J. Fluid Eng.*, Vol. 119, pp. 512~518.

Rogers, Kwak, 1990, "Upwind Differencing Scheme for the Time-accurate Incompressible Navier-Stokes Equations," *AIAA J.*, Vol. 28, No. 2.